Research Article

Ádám Révész*, Dániel G. Fodor, György Krállics, Tony Spassov, and Marcell Gajdics

Structural and hydrogen storage characterization of nanocrystalline magnesium synthesized by ECAP and catalyzed by different nanotube additives

Abstract: Ball-milled nanocrystalline Mg powders catalyzed by TiO_2 powder, titanate nanotubes and carbon nanotubes were subjected to intense plastic deformation by equal-channel angular pressing. Microstructural characteristics of these nanocomposites have been investigated by X-ray diffraction. Microstructural parameters, such as the average crystallite size, the average dislocation density and the average dislocation distance have been determined by the modified Williamson–Hall analysis. Complementary hydrogen desorption and absorption experiments were carried out in a Sieverts' type apparatus. It was found that the Mg-based composite catalyzed by titanate nanotubes exhibits the best overall H-storage performance, reaching 7.1 wt% capacity. The hydrogenation kinetic curves can be fitted by the contracting volume function for all the investigated materials. From the fitted parameters, it is confirmed that the titanate nanotube additive results in far the best kinetic behavior, including the highest hydride front velocity.

Keywords: hydrogen storage, Mg-based microstructure, severe plastic deformation, equal-channel angular pressing

* **Corresponding author: Ádám Révész,** Department of Materials Physics, Eötvös University, P.O.B. 32, H-1518 Budapest, Hungary, e-mail: reveszadam@ludens.elte.hu, fax: +36-1-372-2811
Dániel G. Fodor, Marcell Gajdics: Department of Materials Physics, Eötvös University, P.O.B. 32, H-1518 Budapest, Hungary
György Krállics: Department of Materials Science and Engineering, Budapest University of Technology and Economics, H-1111, Bertalan L. Str. 7, Budapest, Hungary
Tony Spassov: Department of Chemistry, University of Sofia "St.Kl.Ohridski", 1164 Sofia, Bulgaria

1 Introduction

The energy consumption of the Earth is going to be doubled by 2050, which requires the immediate introduction of renewable energy sources to the energy network [1]. Nevertheless, these alternative sources at the moment are barely competitive with conventional fossil fuels [2], and hydrogen as a secondary energy carrier has received constantly increasing attention in the last couple of decades, mainly due to its very high chemical energy ($120–140 \, MJ \cdot kg^{-1}$). In order to overcome the substantial economical and technical challenges, the problem of efficient production and storage needs to be solved [3]. One way to store hydrogen is the atomic absorption by chemisorption in solid metal-based compounds [4–6]. As was demonstrated expansively, solid-state hydrogen storage in metal-based compounds results in higher energy density per mass when compared to molecular storage of the hydrogen gas in high-pressure tanks or to low-temperature liquefaction [7].

Among the large variety of different chemisorbing materials, magnesium-based alloys and compounds have been comprehensively examined because of their high H-storage capacities ($3,700 \, W \cdot h \cdot L^{-1}$ or $2,600 \, W \cdot h \cdot kg^{-1}$), low mass density, nontoxic nature, high abundance and relatively low cost, which allow them to be considered as a potential candidate for future applications [8–11]. Unfortunately, the poor thermodynamics [12], the high enthalpy of the $Mg \leftrightarrow MgH_2$ reaction and the sluggish sorption kinetics below 300°C are the main obstacles that still hamper the wide-spread practical utilization of the Mg–H system [8,9].

In order to eliminate the drawbacks of the hydrogen sorption kinetics of Mg-based alloys, different processing techniques resulting in nanocrystallization of metallic powders have been widely applied to reduce significantly both the particle size of the powders and the coherently scattering crystallite size [5,8,13–16]. Among these methods,

high-energy ball milling (HEBM) is considered to be the most efficient since the high density of lattice defects [15] and increased volume fraction of grain boundaries during the severe plastic deformation (SPD) can significantly enhance the hydrogen diffusion length resulting in improved hydrogen sorption properties [17–21]. Despite the advantages of HEBM, there exist some drawbacks, including high-energy consumption, expensiveness of industrial level production and surface oxidation with consequent potential fire risk. These disadvantages can comprehensively be eliminated by other SPD techniques, resulting in massive bulk samples, including high-pressure torsion (HPT) and equal-channel angular pressing (ECAP). These methods originally were applied for producing impurity and porosity-free massive bulk nanocrystalline samples [22,23]. As has been shown recently, the uniaxial pressure combined with simultaneous torsional straining during the HPT process can significantly improve the hydrogen sorption performance of Mg-based nanocrystalline systems [24–29].

The primary advantages related to ECAP are the production of more air-resistant bulk materials, in comparison to powders produced solely by HEBM [30,31]. In a recent paper, Rabkin et al. provided an overview of the attempts of employing ECAP on different Mg-based systems in order to improve their hydrogen desorption/ absorption performance [32]. It was demonstrated that the increased density of lattice defects in a ZK60 magnesium alloy positively influences the hydrogen desorption pressure and decreases the pressure hysteresis in pressure–composition isotherms [33]. Moreover, the proper combination of ECAP and HEBM techniques can totally eliminate the pressure hysteresis [34]. As was highlighted by Skripnyuk et al., the increase of the equilibrium pressure is associated with the chemical inhomogeneity of the ZK60 alloy [34]. In addition, ECAP can produce special features of commercial purity magnesium for hydrogen sorption such as preferential textures. Faster kinetics, larger capacities and lower sorption temperatures correlate directly with the formation of the (002) texture [35]. The hydrogen storage performance of an AZ31 Mg-alloy can be effectively modified by increasing the ECAP pass number. The best overall behavior was found after applying route B_c for $N = 8$ consecutive passes [36]. The deformation-induced precipitation of the $Mg_{17}Al_{12}$ phase in the Mg-matrix during the ECAP deformation positively affects the H-kinetics of an AZ61 alloy [37]. Numerical simulations combined with experimental microstructural analysis confirmed that the best hydrogen uptake occurs when Mg is subjected to ECAP through route B_c [38].

When ECAP is combined with other SPD methods, such as cold rolling [39–41] or accumulated roll-bonding [42], the microstructure undergoes an additional refinement promoting the formation of extra favorable sites for H-absorption. Based on the results on Mg-based systems processed by the combination of different SPD methods, it is concluded that the amount of equivalent strain achieved after the deformation process, the deformation geometry, and the resulting nanostructure and microstructure are together responsible for the ultimate H-storage behavior [43]. The long-term durability of the ZK60 alloy processed by ECAP was confirmed through 1,000 absorption–desorption cycles with almost zero deterioration in the achieved capacity [44]. It was found that the multipass ECAP process of an Mg–Ni alloy at elevated temperature results in the evolution of a two phase ($Mg + Mg_2Ni$) microstructure, which significantly accelerates the kinetics of hydrogenation and increase the equilibrium hydrogen pressure, in correlation with the chemical inhomogeneity formed during deformation [45].

Recently, we investigated the influence of simultaneous mixing of transition metal oxide and multiwall carbon nanotube (MWCNT) catalysts on the hydrogenation behavior of severely deformed nanocrystalline Mg by HPT [46,47]. The hint of the present research is to replace these two types of catalyst additives by applying only metal-oxide-based nanotubes prepared from TiO_2 and investigate its effect on the sorption properties of Mg prepared by the combined method of HEBM and ECAP. For comparison, magnesium samples catalyzed with TiO_2 powder and with TiO_2 and MWCNTs were also synthesized.

2 Experimental

2.1 Sample preparation

2.1.1 Preparation of titanate nanotubes

Titanate nanotubes (TNs) were prepared via the microwave-assisted hydrothermal method [48,49]. The starting material was anatase TiO_2 powder (supplied by Reanal; purity 99.9%), which was mixed with 10 mol NaOH aqueous solution. The suspension was stirred ultrasonically and then the mixture was subjected to microwave irradiation in a Monowave 300 microwave reactor. The product was then dispersed in distilled water and centrifuged. The remaining material was dried at 60°C. Figure 1 shows a typical transmission electron micrograph (taken on a JEOL JEM 3010 HR-TEM equipped with a LaB6 cathode) of
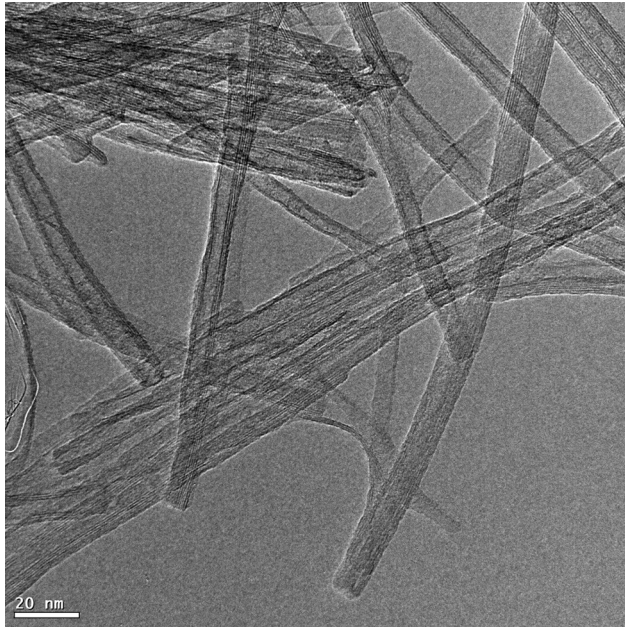
Figure 1: TEM micrograph of the as-synthesized titanate nanotubes.

the as-prepared TNs. As seen, these TNs are multiwall tubes, with a length ranging from 50 nm to a few hundred nanometers and their diameter is in the range of 10 nm. The details of the synthesis and microstructural analysis of the as-prepared TNs have already been published elsewhere [50].

2.1.2 Synthesis of Mg-based nanocomposites

Nanocrystalline Mg and Mg-based composites were prepared by HEBM in a SPEX 8000 M Mixer Mill using a stainless steel vial (volume: 65 mL). The powders were milled using 10 stainless steel balls (1/4 in.) with an RPM of 1,425, while the ball-to-powder weight ratio was chosen as 10:1. Sample manipulation was carried out in a glove box, and HEBM was processed in an argon atmosphere in order to minimize the oxidation of the powder samples.

For reference, pure magnesium (Sigma-Aldrich; purity 99.9%) was milled for 3 h (denoted Mg). When 5 wt% TiO_2 powder (Sigma-Aldrich; purity 99.8%) was milled together with the Mg powder, the milling time was chosen again as 3 h (Mg + TiO_2). Since MWCNTs and TNs are vulnerable to milling for long times [50], they can only be milled for a relatively short milling time. For the composite containing 2.5 wt% TiO_2 powder and 2.5 wt% MWCNTs (Sigma-Aldrich; purity 98%, outer diameter: 6–13 nm, length: 2.5–20 µm), magnesium was premilled with

Figure 2: Photographs taken on the capsules (a) before and (b) after the ECAP deformation.

TiO_2 for 2½ h and then an additional ½ h milling together with the nanotube catalysts were applied (Mg + TiO_2 + CNT). The milling sequence of the sample catalyzed by 5 wt% TN (Mg + TN) included a 2½ h long pre-milling of Mg, which subsequently was milled together with TNs for an extra ½ h. For all samples, 3 mL of n-hexane was also added to prevent excessive agglomeration of Mg during milling.

2.1.3 ECAP

For subsequent ECAP processing, the milled nanocomposites were compacted into pastilles with a diameter of 10 mm and height of 4 mm under a hydraulic pressure of 1 GPa. Then, ten of these as-compacted billets were stuck and encapsulated together in a cylindrical

aluminum tube (diameter: 16 mm, height: ~100 mm); see Figure 2a. The ECAP procedure has been performed at room temperature using a solid die with an internal channel angle of $\Phi = 90°$ and an angle of the outer curvature of the two parts of the die $\psi = 30°$ [23]. For our experiments, four repetitive pressings have been carried out for each tube using route "A" without any rotation between the subsequent passages [23]. The photographs taken on the deformed tubes can be seen in Figure 2b. For further characterization, the Al tubes have been mechanically removed and slices of the remaining Mg-based composites were cut.

2.2 Microstructural characterization

The overall microstructure of ECAP-processed specimens was examined by X-ray powder diffraction (XRD). The measurements were carried out on a Rigaku SmartLab diffractometer in $\theta-2\theta$ geometry using Cu-Kα radiation ($\lambda = 0.154$ nm). The X-ray photons were collected from 20° to 75° with a step size of 0.01°. The recorded X-ray diffraction profiles have been evaluated by the modified Willamson–Hall procedure [51,52]. In brief, the broadening of the crystalline Bragg peaks can be given by the sum of a size and a strain term:

$$\Delta K = \Delta K^{SIZE} + \Delta K^{STRAIN} = 0.9/D_{WH}$$
$$+ (\pi M^2 b^2/2)^{1/2} \rho^{1/2}(K\bar{C}^{1/2}) + O(K^2\bar{C}), \tag{1}$$

where $K = 2\sin\theta/\lambda$ and $\Delta K = 2\cos\theta(\Delta\theta)/\lambda$ with θ and $\Delta\theta$ being the position and full width at half-maximum of the Bragg reflections. The ΔK^{SIZE} term is proportional to the inverse of the coherently scattering average crystallite size (D_{WH}). In this model, the strain broadening (ΔK^{STRAIN}) is caused by the strain anisotropy of dislocations, whose Burgers vector and density are denoted by b and ρ, respectively. The constant M describes the strength of correlation between the dislocations and $M\sim3$ for a restrictedly random dislocation population. Here, $\bar{C}$ is the so-called average contrast factor of dislocations, referring to the anisotropic nature of their strain broadening. For hexagonal crystals, $\bar{C}$ can be given as [53]

$$\bar{C} = C_{hk0}(1 + q_1 x + q_2 x^2), \tag{2}$$

where $x = (2/3)(l/Ka)^2$. Here, l is the last Miller index of the hexagonal lattice plane and a is the lattice parameter in the basal plane. For hexagonal Mg, $C_{hk0} = 0.19483$, $q_1 = 0.067864$ and $q_2 = -0.19759$ [53].

2.3 Hydrogenation experiments

The hydrogenation behavior of the ECAP samples was examined in a home-made Sievers'-type apparatus. Volumetric calibration of the equipment was performed by an external reservoir using the van der Waals equation of gases. Isotherm measurements were carried out at 573 K (±5 K), with an initial hydrogen pressure of 1 MPa. Heating up to 573 K was performed in a vacuum, followed by the insertion of hydrogen into the sample chamber. The preset hydrogen pressure was reached in a few seconds. Several consecutive absorption–desorption cycles were carried out before the actual absorption measurement. For each measurement, approximately 100 mg of the material was used. The uncertainty of the measurement is about 0.03 wt%.

3 Results and discussion

The logarithmic XRD patterns of ECAP-processed materials are visualized in Figure 3. As expected, the dominant constituent phase is hexagonal Mg for all samples. In addition, the (411) reflection of TiO_2 can also be recognized for the Mg + TiO_2 and Mg + TiO_2 + CNT composites. On the other hand, no reflection corresponding to MWCNTs and TNs can be seen in either nanotube containing samples (Mg + TiO_2 + CNT and Mg + TN), which is correlated to the low crystallinity of these tube-shaped additives. Another explanation could be partial amorphization, which might
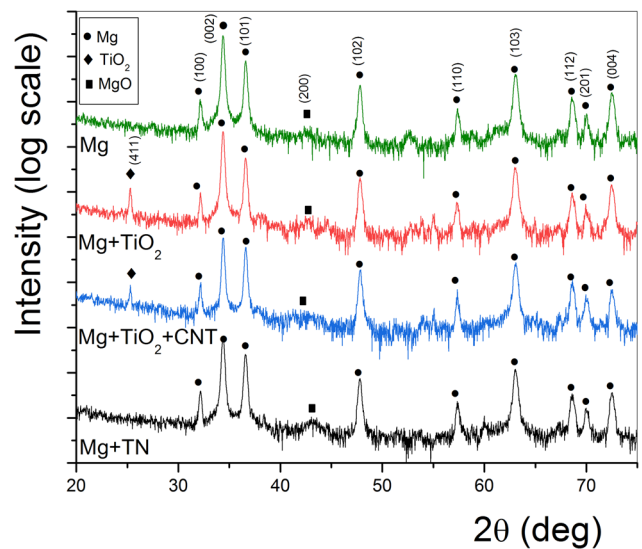

Figure 3: XRD patterns of the catalyzed Mg-based composites.

occur during the HEBM process when the milling balls impact the tubes [50]. At the same time, a very low-intensity peak of MgO is present at around $2\theta = 43°$ for all the ECAP-processed samples.

The relative intensities of the hexagonal Mg peaks undergo a drastic change after the plastic deformation by ECAP. Notably, the intensity ratios of the most intensive (101) and (002) reflections are generally regarded as a measure of texture generated during the different deformation processes [46]. As one compares the $\eta = I(101)/I(002)$ ratios obtained directly from the XRD patterns with the literature value ($\eta = 2.78$ [54]), it is recognized that the combined HEBM + ECAP results in drastic changes, i.e., η is below 0.6 for all the four samples, reaching a minimum value $\eta = 0.26$ for the Mg + TiO$_2$ composite. Consequently, it is concluded that a significant (002) texture develops after the ECAP process for all the investigated composites; however, its magnitude varies with the type of the catalysts, namely the MWCNT and TN additives result in a somewhat weaker texture.

Figure 4 presents the lattice parameters of the hexagonal Mg phase calculated from the fitted XRD peak positions. Regarding the pure Mg sample as well as the composite materials, it is seen that both lattice parameters (*a* and *c*) behave similarly. Namely, the lattice parameter *a* is fairly close to the literature value (marked by horizontal dashed line), while the *c* parameter is consistently smaller (~0.03% decrease); however, the magnitude of the difference is roughly equal to the experimental error. In hexagonal close-packed structure, the easiest slip occurs in the basal plane by the formation of <*a*>-type dislocations, which affects the lattice parameter *a* [55]. Since the deviation of *a* from the literature

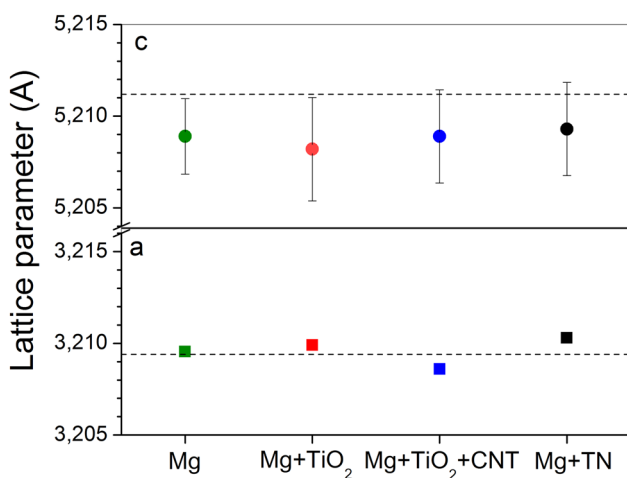value is negligible for all the samples, we can assume that severe plastic deformation generated during the ECAP process does not promote significantly the formation of this type of lattice defects, in contrast to the HPT of similar Mg-based composites [46]. The underlying mechanism of the decrease in the *c* parameter and the consequent shrinkage of the close-packed hexagonal unit cell is not fully understood; however, it might be assumed that during the SPD deformation of the combined HEBM + ECAP processes, an intensive formation of fresh grain boundaries takes place, which is abundant in distorted atomic bonds [56].

Figure 5a presents the ΔK values of the strongest five magnesium Bragg reflections as a function of K for all the ECAP-processed samples (classical Williamson–Hall method [57]). The gradual increase of ΔK with K evidently corresponds to the presence of lattice distortions; however, the observed systematic deviation from the linear correlation indicates significant strain anisotropy. On the
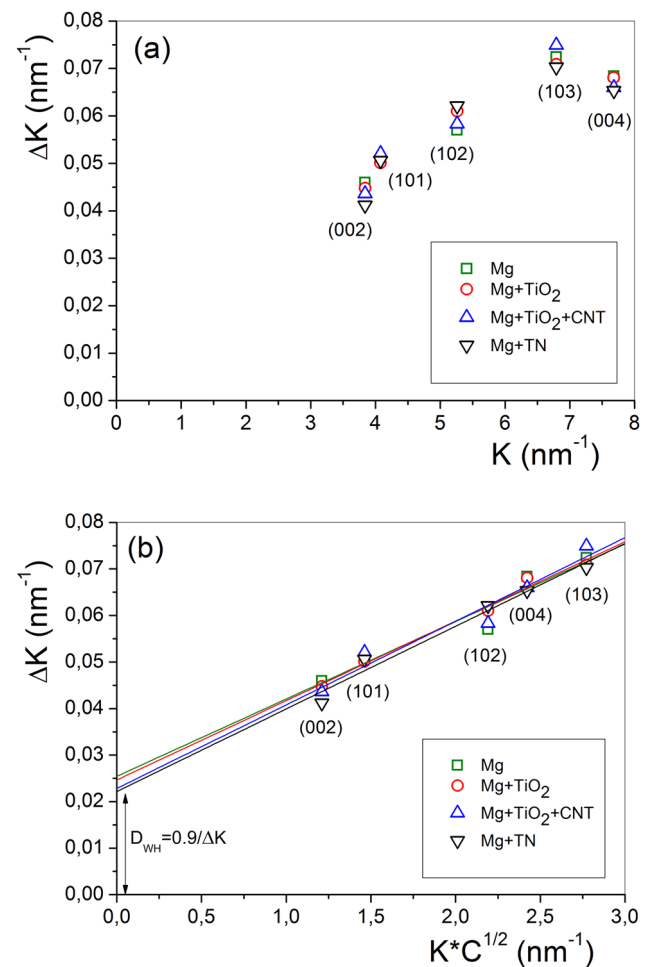

Figure 4: Mg lattice parameters (*a* and *c*) of the Mg-based composites. Dashed lines indicate the literature value.

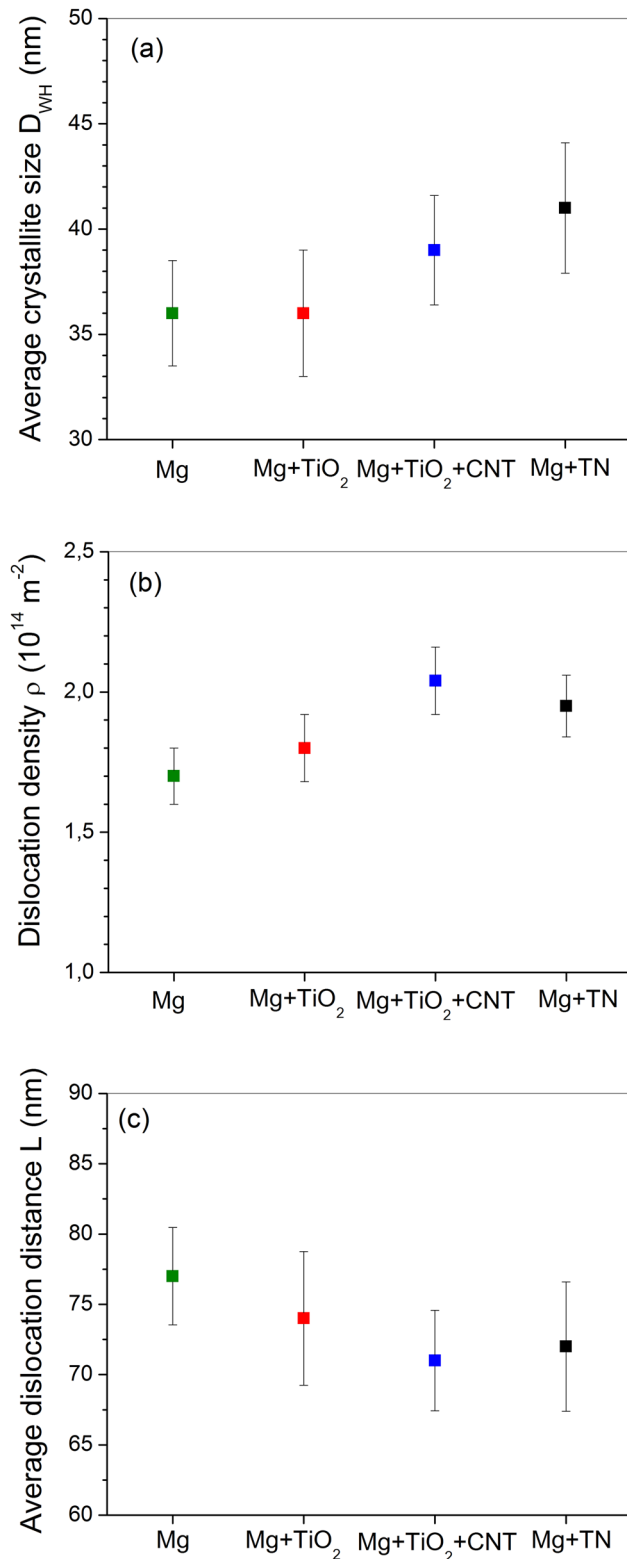**Figure 5:** (a) Classical and (b) modified Williamson–Hall plots.

Figure 6: Microstructural parameters (a) average crystallite size, (b) dislocation density and (c) average dislocation distance obtained from the modified Williamson–Hall analysis.

other hand, the modified Williamson–Hall plots in Figure 5b confirm that, according to equation (1), the proper scaling parameter is $K\bar{C}^{1/2}$ instead of K, which undoubtedly supports the presence of dislocations. The intercept of the fitted straight lines at $K = 0$ yields D_{WH}. As one can recognize, only a small variation takes place in D_{WH} values of hexagonal magnesium when it is milled together with different additives (see Figure 6a), and the combined HEBM + ECAP procedure results in a significant nanocrystallization with average crystallite size in the 36–41 nm range. The smallest values are obtained for pure Mg and Mg + TiO$_2$. When a premilling of Mg was applied, the final crystallite size is somewhat larger, i.e., 39 nm for Mg + TiO$_2$ + CNT and 41 nm for the Mg + TN composites. Figure 6b presents the variation of the average dislocation density for the different ECAP-processed samples. As can be seen, severe plastic deformation promotes high-density values reaching $\rho \sim 10^{14}\,m^{-2}$ for all samples. The highest values (2.0×10^{14} and $1.95 \times 10^{14}\,m^{-2}$) were achieved for the composites containing nanotube additives. These values are one order of magnitude higher than that was developed for ball-milled Mg powder [58], indicating the extreme intensity of plastic deformation during ECAP. On the other hand, when Mg-based composites containing TNs were exposed to HPT, the final values can reach $\rho \sim 10^{15}\,m^{-2}$ [50]. The observed slightly higher D_{WH} and ρ values for the nanotube containing Mg + TiO$_2$ + CNT and Mg + TN samples might correspond to the different HEBM routes and different mechanical properties of MWCNTs and TNs compared to the TiO$_2$ powder. In addition, the calculated average defect distance, $L = \rho^{-1/2}$ ($L = $ 71–77 nm) exceeds D_{WH} by a factor of ~2 for all investigated samples (Figure 6c). Despite the relatively high dislocation density, it means that ~85% of the crystallites can be considered defect-free.

Hydrogenation kinetic curves of the different magnesium-based composites obtained at 573 K are presented in Figure 7. It is noted that all the ECAP-processed samples absorb hydrogen after one dehydrogenation–hydrogenation activation cycle, thereafter the maximum storage capacity is reached. For plastically deformed Mg, the obtained value is 6.6 wt% (see also Table 1) after 4,200 s of sorption. When Mg is catalyzed by TNs, the achieved capacity increases above 7 wt%, reaching almost the theoretical limit considering that the amount of the additive is 5 wt% in the sample. This value considerably exceeds the H-storage capacity of the same titanate-catalyzed composite prepared by HPT [50], most probably due to the unavoidable exposure to air during the torsion process. If one
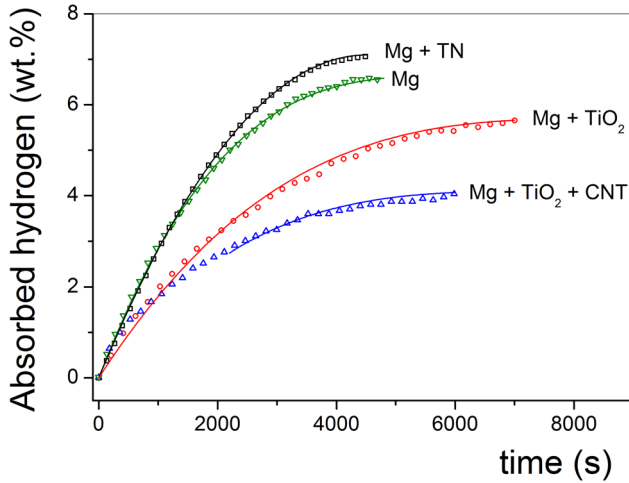
Figure 7: Absorption kinetic curves of the Mg-based composites processed by ECAP.

compares these results with the recently published research in the literature, it is concluded that TN-catalyzed Mg possesses slightly better hydrogen absorption capacity than ball-milled magnesium doped by carbon-supported TiO$_2$ [59]. As also recognized from Table 1, the initial hydrogenation is rather fast for the pure Mg and Mg-based composites catalyzed by nanotubes, absorbing 1.27–1.52 wt% hydrogen after 500 s, while the kinetics is a bit more sluggish when TiO$_2$ powder was milled to Mg. Nonetheless, the subsequent sorption behavior is different, i.e., a saturation at a significantly lower capacity value is detected not only for the Mg + TiO$_2$ composite (5.7 wt%) but also for the Mg + TiO$_2$ + CNT alloy (4.1 wt%). These different kinetic performances of the catalyzed Mg-based composites cannot be explained satisfactorily by the microstructural features of these materials since the difference of D_{WH} and ρ values is insignificant as is demonstrated in Figure 6a and b. Therefore it is suggested that the catalytic effect of the different additives itself can be responsible for the observed H-storage behaviors. It is worth noting that the obtained initial absorption rate determined

as the tangent of the fitted straight line to the normalized hydrogenation curves at $t = 0$ for all the ECAP-processed samples ($>2.4 \times 10^{-3}$ wt%·s^{-1}) are better when it is compared to HPT-deformed composites [46], referring to the enhanced formation of diffusion paths to the available H-sites by the ECAP technique.

In order to characterize the hydrogenation behavior of the Mg-based composites, the absorption curves have been fitted by the contracting volume (CV) function [60]. In brief, this kinetics is fulfilled when the nucleation commences on the surface of the crystallites and growth takes place from the surface into the bulk, resulting in the formation of a new hydride phase with a constant interface velocity. This kind of kinetics can be described by

$$\alpha_{CV}(t, R) = 1 - (1 - k_{CV}t)^n, \qquad (3)$$

where k_{CV} is a reaction constant and is given as $k_{CV} = U/R$, where U is the velocity of the hydride–metal interface motion and $R = 0.5D_{WH}$ is the average crystallite radius. n depends on the dimensionality of the growth. The obtained k, U, and n values are listed in Table 1. It is noted that the entire kinetic curve of the Mg + TiO$_2$ + CNT composite cannot be fitted satisfactorily by a single CV function, therefore the corresponding values are only valid for the 2,300–6,000 s interval. As it is evident from Table 1, the titanate-catalyzed composites exhibit far the best kinetic parameters ($k = 2.2 \times 10^{-4}$ s^{-1} and $U = 4.50 \times 10^{-3}$ nm·s^{-1}), which indicate that the hydrogen dissociation, diffusion, and the growth of the hydride phase are propelled by the special morphological features by the TNs [50], exhibiting more porous structure, in comparison with TiO$_2$ powder or TiO$_2$ + CNT. In addition, these values are comparable to those obtained for nanocrystalline Mg processed by other SPD techniques [61]. As also seen, the dimensionality of growth ranges from $n = 2$ to 3 for all the ECAP-deformed samples, which indicates that the propagation of interphase boundary is isotropic for pure Mg, Mg + TiO$_2$, and Mg + TiO$_2$ + CNT, while anisotropic for the Mg + TN alloy.

Table 1: Maximum absorbed hydrogen, initial sorption rate, and the fitted parameters of the CV model

Sample	Total absorbed hydrogen (wt%)	Absorbed hydrogen at 500 s (wt%)	CV reaction constant [k] (10^{-4} s^{-1})	Hydride front velocity [U] (10^{-3} nm·s^{-1})	CV exponent [n]
Mg	6.6	1.52	1.66	2.99	3.08
Mg + TiO$_2$	5.7	1.03	1.14	2.05	3.12
Mg + TiO$_2$ + CNT	4.1	1.27	1.29	2.51	3.32
Mg + TN	7.1	1.42	2.20	4.50	2.04

4 Conclusion

In this research, the HEBM + ECAP deformation route was applied on nanocrystalline magnesium catalyzed by TiO_2 powder, TiO_2 together with MWCNTs and TNs. The modified Williamson–Hall analysis of the X-ray Bragg reflections revealed that this deformation process results in a nanocrystallization, reaching a minimum value of D_{WH} ~36 nm for Mg. At the same time, a remarkable (002) texture develops in the hexagonal lattice structure for all the investigated composites. The average dislocation density reaches high values ($\rho \sim 10^{14}\,m^{-2}$), referring to an intensive plastic deformation occurring during HEBM and subsequent ECAP. The hydrogen absorption measurements confirmed that the TN-catalyzed Mg-based composite exhibits the best overall H-storage performance, reaching 7.1 wt% capacity, close to the theoretical value. The kinetic curves of hydrogenation can satisfactorily be fitted by the contracting volume (CV) function. From the fitted parameters, it is undoubtedly confirmed that the Mg + TN composite exhibits far the best kinetic parameters, including the highest hydride front velocity ($U = 4.50 \times 10^{-3}\,nm \cdot s^{-1}$).

Author contributions: Á. Révész: powder processing, X-ray data evaluation, methodology, supervision, writing the manuscript; D. G. Fodor: X-ray data evaluation; G. Krállics: ECAP sample preparation; T. Spassov: H-kinetics measurements; M. Gajdics: Nanotube preparation, XRD measurements, HRTEM study.

Conflict of interest: The authors declare no conflict of interest. The funders had no role in the design of the study; in the collection, analyses, or interpretation of data; in the writing of the manuscript, or in the decision to publish the results.

References

[1]   Sahaym, U. and M. G. Norton. Advances in the application of nanotechnology in enabling a hydrogen economy. *Journal of Materials Science*, Vol. 43, 2008, pp. 5395–5429.

[2]   Ren, J., N. M. Musyoka, H. W. Langmi, M. Mathe, and S. Liao. Current research trends and perspectives on materials-based hydrogen storage solutions: a critical review. *International Journal of Hydrogen Energy*, Vol. 42, 2017, pp. 289–311.

[3]   Borgschulte, A. The hydrogen grand challenge. *Frontiers in Energy Research*, Vol. 4, 2016, id. 11.

[4]   Schlabach, L. and A. Zuttel. Hydrogen-storage materials for mobile applications. *Nature*, Vol. 414, 2001, pp. 353–358.

[5]   Varin, R. A., T. Czujko, Z. S. Wronski. *Nanomaterials for solid state hydrogen storage*, Springer, New York, NY, USA, 2009.

[6]   Niaz, S., T. Manzoor, and A. H. Pandith. Hydrogen storage: materials, methods and perspectives. *Renewable and Sustainable Energy Reviews*, Vol. 50, 2015, id. 50.

[7]   Rusman, N. A. A. and M. Dahari. A Review on the current progress of metal hydrides material for solid-state hydrogen storage applications. *International Journal of Hydrogen Energy*, Vol. 41, 2016, pp. 12108–12126.

[8]   Aguey-Zinsou, K.-F. and J. R. Ares-Fernández. Hydrogen in magnesium: new perspectives toward functional stores. *Energy & Environmental Science*, Vol. 3, 2010, pp. 526–543.

[9]   Pasquini, L. The effect of nanostructure on the hydrogen sorption properties of magnesium-based metallic compounds: A review. *Crystals*, Vol. 8, 2018, id. 106.

[10] Luo, Q., J. Li, B. Li, B. Liu, H. Shao, and Q. Li. Kinetics in Mg-based hydrogen storage materials: enhancement and mechanism. *Journal of Magnesium Alloys*, Vol. 7, 2019, pp. 58–71.

[11] Crivello, J.-C., B. Dam, R. V. Denys, M. Dornheim, D. M. Grant, J. Huot, et al. Review of magnesium hydride-based materials: development and optimization. *Applied Physics A*, Vol. 122, 2016, id. 97.

[12] Wang, H., H. J. Lin, W. T. Cai, L. Z. Ouyang, and M. Zhu. Tuning kinetics and thermodynamics of hydrogen storage in light metal element based systems – A review of recent progress. *Journal of Alloys and Compounds*, Vol. 658, 2016, pp. 280–300.

[13] Sadhasivam, T., H.-T. Kim, S. Jung, S.-H. Roh, J.-H. Park, and H.-Y. Jung. Dimensional effects of nanostructured Mg/MgH₂ for hydrogen storage applications. *Renewable and Sustainable Energy*, Vol. 72, 2017, pp. 523–534.

[14] Fátay, D., Á. Révész, and T. Spassov. Particle size and catalytic effect on the dehydriding of MgH₂. *Journal of Alloys and Compounds*, Vol. 399, 2005, pp. 237–241.

[15] Révész, Á. and D. Fátay. Microstructural evolution of ball-milled MgH₂ during a complete dehydrogenation–hydrogenation cycle. *Journal of Power Sources*, Vol. 195, 2010, pp. 6997–7002.

[16] Fátay, D., T. Spassov, P. Delchev, G. Ribárik, and Á. Révész. Microstructural development in nanocrystalline MgH₂ during H-absorption/desorption cycling. *International Journal of Hydrogen Energy*, Vol. 32, 2007, pp. 2914–2919.

[17] Polanski, M., J. Bystrzycki, and T. Plocinski. The effect of milling conditions on microstructure and hydrogen absorption/desorption properties of magnesium hydride (MgH_2) without and with Cr_2O_3 nanoparticles. *International Journal of Hydrogen Energy*, Vol. 33, 2008, pp. 1859–1867.

[18] Novakovic, J. G., N. Novakovic, S. Kurko, S. M. Govedarovic, T. Pantic, B. P. Mamula, et al. Influence of defects on the stability and hydrogen-sorption behavior of Mg-based hydrides. *ChemPhysChem*, Vol. 20, 2019, pp. 1216–1247.

[19] Huot, J. *Enhancing hydrogen storage properties of metal hybrids*, Springer Nature, Switzerland, 2016.

[20] Pasquini, L. Design of nanomaterials for hydrogen storage. *Energies*, Vol. 13, 2020, id. 3503.

[21] Leiva, D. R., Jorge Jr. A. M., T. T. Ishikawa, and W. J. Botta. Hydrogen storage in Mg and Mg-based alloys and composites processed by severe plastic deformation. *Materials Transactions*, Vol. 60, 2019, pp. 1561–1570.

[22] Valiev, R. Z., R. K. Ishlamgaliev, and I. V. Alexandrov. Bulk nanostructured materials from severe plastic deformation. *Progress in Materials Science*, Vol. 45, 2000, pp. 103–89.

[23] Valiev, R. Z. and T. G. Langdon. Principles of equal-channel angular pressing as a processing tool for grain refinement. *Progress in Materials Science*, Vol. 51, 2006, pp. 881–981.

[24] Révész, Á. and M. Gajdics. High-pressure torsion of non-equilibrium hydrogen storage materials: a review. *Energies*, Vol. 14, 2021, id. 819.

[25] Kusadome, Y., K. Ikeda, Y. Nakamori, S. Orimo, and Z. Horita. Hydrogen storage capability of $MgNi_2$ processed by high pressure torsion. *Scripta Materialia*, Vol. 57, 2007, pp. 751–753.

[26] Révész, Á., Z. Kánya, T. Verebélyi, P. J. Szabó, A. P. Zhilyaev, and T. Sapssov. The effect of high-pressure torsion on the microstructure and hydrogen absorption kinetics of ball-milled $Mg_{70}Ni_{30}$. *Journal of Alloys and Compounds*, Vol. 504, 2010, pp. 83–88.

[27] Hongo, T., K. Edalati, M. Arita, J. Matsuda, E. Akiba, and Z. Horita. Significance of grain boundaries and stacking faults on hydrogen storage properties of Mg_2Ni intermetallics processed by high-pressure torsion. *Acta Materialia*, Vol. 92, 2015, pp. 46–54.

[28] Gajdics, M., M. Calizzi, L. Pasquini, E. Schafler, and Á. Révész. Characterization of a nanocrystalline Mg–Ni alloy processed by high-pressure torsion during hydrogenation and dehydrogenation. *International Journal of Hydrogen Energy*, Vol. 41, 2016, pp. 9803–9809.

[29] Révész, Á., M. Gajdics, E. Schafler, M. Calizzi, and L. Pasquini. Dehydrogenation-Hydrogenation characteristics of nanocrystalline Mg_2Ni powders compacted by high-pressure torsion. *Journal of Alloys Compounds*, Vol. 702, 2017, pp. 84–91.

[30] Jorge, A. M., E. Prokofiev, G. Ferreira de Lima, E. Rauch, M. Veron, W. J. Botta, et al. An investigation of hydrogen storage in a magnesium-based alloy processed by equal-channel angular pressing. *International Journal of Hydrogen Energy*, Vol. 38, 2013, pp. 8306–8312.

[31] Wang, L., J. Jiang, A. Ma, Y. Li, and D. Song. A critical review of Mg-based hydrogen storage materials processed by equal channel angular pressing. *Metals*, Vol. 7, 2017, id. 324.

[32] Rabkin, E., V. Skripnyuk, and Y. Estrin. Ultrafines-grained magnesium alloys for hydrogen storage obtained by severe plastic deformation. *Frontiers in Materials*, Vol. 6, 2019, id. 240.

[33] Skripnyuk, V. M., E. Rabkin, Y. Estrin, and R. Lapovok. Improving hydrogen storage properties of magnesium based alloys by equal channel angular pressing. *International Journal of Hydrogen Energy*, Vol. 34, 2009, pp. 6320–6324.

[34] Skripnyuk, V. M., E. Rabkin, Y. Estrin, and R. Lapovok. The effect of ball milling and equal channel angular pressing on the hydrogen absorption/desorption properties of Mg-4.95 wt% Zn-0.71 wt% Zr (ZK60) alloy. *Acta Materialia*, Vol. 52, 2004, pp. 405–414.

[35] Jorge, A. M., G. Ferreira de Lima, M. R. Martins Triques, W. J. Botta, C. S. Kiminami, R. P. Nogueira, et al. Correlation between hydrogen storage properties and textures induced in magnesium through ECAP and cold rolling. *International Journal of Hydrogen Energy*, Vol. 39, 2014, pp. 3810–3821.

[36] Chiu, C., S.-J. Huang, T.-Y. Chou, and E. Rabkin. Improving hydrogen storage performance of AZ31 Mg alloy by equal channel angular pressing and additives. *Journal of Alloys and Compounds*, Vol. 743, 2018, pp. 437–447.

[37] Huang, S.-J., C. Chiu, T.-Y. Chou, and E. Rabkin. Effect of equal channel angular pressing (ECAP) on hydrogen storage properties of commercial magnesium alloy AZ61. *International Journal of Hydrogen Energy*, Vol. 43, 2018, id. 4380.

[38] Skryabina, N., V. Aptukov, P. Romanov, D. Fruchart, P. de Rango, G. Girard, et al. Microstructure optimization of Mg-alloys by the ECAP process including numerical simulation, SPD treatments, characterization, and hydrogen sorption properties. *Molecules*, Vol. 24, 2018, id. 89.

[39] Soyama, J., R. Floriano, D. R. Leiva, Y. Guo, A. M. Jorge Junior, E. Pereira da Silva, et al. Severely deformed ZK60 + 2.5% Mm alloy for hydrogen storage produced by two different processing routes. *International Journal of Hydrogen Energy*, Vol. 41, 2016, pp. 11284–11292.

[40] Jorge Jr., A. M., E. Prokofiev, M. R. M. Triques, V. Roche, W. J. Botta, C. S. Kiminami, et al. Effect of cold rolling on the structure and hydrogen properties of AZ91 and AM60D magnesium alloys processed by ECAP. *International Journal of Hydrogen Energy*, Vol. 42, 2017, pp. 21822–21831.

[41] Lima, G. F., M. R. M. Triques, C. S. Kiminami, W. J. Botta, and A. M. Jorge. Hydrogen storage properties of pure Mg after the combined processes of ECAP and cold-rolling. *Journal of Alloys and Compounds*, Vol. 586, 2014, pp. S405–S408.

[42] Asselli, A. A. C., D. R. Leiva, J. Huot, M. Kawasaki, T. G. Langdon, and W. J. Botta. Effects of equal-channel angular pressing and accumulative roll-bonding on hydrogen storage properties of a commercial ZK60 magnesium alloy. *International Journal of Hydrogen Energy*, Vol. 40, 2015, pp. 16971–16976.

[43] Révész, Á., M. Gajdics, L. K. Varga, Gy Krállics, L. Péter, and T. Spassov. Hydrogen storage of nanocrystalline Mg-Ni alloy processed by equal-channel angular pressing and cold rolling. *International Journal of Hydrogen Energy*, Vol. 39, 2014, pp. 9911–9917.

[44] Krystian, M., M. J. Zehetbauer, H. Kropik, B. Mingler, and G. Krexner. Hydrogen storage properties of bulk nanostructured ZK60 Mg alloy processed by equal channel angular pressing. *Journal of Alloys and Compounds*, Vol. 509, 2011, pp. S449–S455.

[45] Skripnyuk, V., V. Buchman, E. Rabkin, E. Estrin, Y. Popov, and M. S. Jorgensen. The effect of equal channel angular pressing on hydrogen storage properties of a eutectic Mg–Ni alloy. *Journal of Alloys and Compounds*, Vol. 436, 2007, pp. 99–106.

[46] Gajdics, M., T. Spassov, V. K. Kis, E. Schafler, and Á. Révész. Microstructural and morphological investigations on Mg-Nb_2O_5-CNT nanocomposites processed by high-pressure torsion for hydrogen storage applications. *International Journal of Hydrogen Energy*, Vol. 45, 2020, pp. 7917–7928.

[47] Révész, Á., T. Spassov, V. K. Kis, E. Schafler, and M. Gajdics. The influence of preparation conditions on the hydrogen sorption of Mg-Nb_2O_5-CNT produced by ball milling and subsequent high-pressure torsion. *Journal of Nanoscience and Nanotechnology*, Vol. 20, 2020, pp. 4587–4590.

[48] Wu, X., Q.-Z. Jiang, Z.-F. Ma, M. Fu, and W.-F. Shangguan. Synthesis of titania nanotubes by microwave irradiation. *Solid State Communications*, Vol. 136, 2005, pp. 513–517.

[49] Wong, C. L., Y. N. Tan, and A. R. Mohamed. A review on the formation of titania nanotube photocatalysts by hydrothermal treatment. *Journal of Environmental Management*, Vol. 92, 2011, pp. 1669–1680.

[50] Gajdics, M., T. Spassov, V. Kovács Kis, F. Beke, Z. Novák, E. Schafler, et al. Microstructural investigation of nanocrystalline hydrogen-storing Mg-titanate nanotube composites processed by high-pressure torsion. *Energies*, Vol. 13, 2020, id. 563.

[51] Ungár, T. and A. Borbély. The effect of dislocation contrast on x-ray line broadening: A new approach to line profile analysis. *Applied Physics Letters*, Vol. 69, 1996, id. 3173.

[52] Révész, Á., T. Ungár, A. Borbély, and J. Lendvai. Dislocations and grain size in ball-milled iron powder. Vol. 7, 1996, pp. 779–788.

[53] Dragomir, I. C. and T. Ungár. Contrast factors of dislocations in the hexagonal crystal system. *Journal of Applied Crystallography*, Vol. 35, 2002, pp. 556–564.

[54] JCPDS Card 35-0821

[55] Hull, D., D. J. Bacon. *Introduction to dislocations*, 5th edn, Butterworth-Heinemann, Elsevier, 2011.

[56] Suryanarayana, C. Mechanical alloying and milling. *Progress in Materials Science*, Vol. 46, 2001, pp. 1–184.

[57] Williamson, G. K. and W. H. Hall. X-ray line broadening from filed aluminium and wolfram. *Acta Metallurgica*, Vol. 1, 1953, pp. 22–31.

[58] Révész, Á. and D. Fátay. Microstructural evolution of ball-milled MgH_2 during a complete dehydrogenation-hydrogenation cycle. *Journal of Power Sources*, Vol. 195, 2010, pp. 6997–7002.

[59] Zhang, X., Z. Leng, M. Gao, J. Hu, F. Du, J. Yao, et al. Enhanced hydrogen storage properties of MgH_2 catalyzed with carbon supported nanocrystalline TiO_2. *Journal of Power Sources*, Vol. 398, 2018, pp. 183–192.

[60] Jacobs, P. W. M. and F. C. Tompkins. Classification and theory of solid reactions. *Chemistry of the solid state*, W. E. Garner, (ed.), Butterworth, London, 1955, pp. 184–212.

[61] Révész, Á. and M. Gajdics. Correlation between microstructure and hydrogen storage properties of nanocrystalline magnesium subjected to high-pressure torsion. *Materials Science Forum*, Vol. 885, 2017, pp. 67–73.